

# Depth of Field Analysis for Multilayer Automultiscopic Displays

D. Lanman, G. Wetzstein, M. Hirsch, and R. Raskar

MIT Media Lab, 75 Amherst Street, Cambridge MA 02139, USA

E-mail: dlanman@media.mit.edu

**Abstract.** With the re-emergence of stereoscopic displays, through polarized glasses for theatrical presentations and shuttered liquid crystal eyewear in the home, automultiscopic displays have received increased attention. Commercial efforts have predominantly focused on parallax barrier and lenticular architectures applied to LCD panels. Such designs suffer from reduced resolution and brightness. Recently, multilayer LCDs have emerged as an alternative supporting full-resolution imagery with enhanced brightness and depth of field. We present a signal-processing framework for comparing the depth of field for conventional automultiscopic displays and emerging architectures comprising multiple light-attenuating layers. We derive upper bounds for the depths of field, indicating the potential of multilayer configurations to significantly enhance resolution and depth of field, relative to conventional designs.

## 1. Introduction

Thin displays that present the illusion of depth have become a driving force in the consumer electronics and entertainment industries, offering a differentiating feature in a market where the utility of increasing 2D resolution has brought diminishing returns. In such systems, binocular depth cues are achieved by presenting different images to each of the viewer's eyes. Automultiscopic displays present such view-dependent imagery without requiring special eyewear, providing both binocular and motion parallax cues. Conventional designs use either light-attenuating parallax barriers, introduced by Ives in 1903 [1], or refracting lens arrays (also known as integral imaging), introduced by Lippmann in 1908 [2]. In both cases, an underlying 2D display is covered with a second optical element. For barrier designs, a second light-attenuating layer is placed slightly in front of the first, whereas lens arrays are directly affixed to the underlying display. In most commercial systems either parallax barriers or lenticular sheets are used for horizontal-only parallax. However, pinhole arrays or integral lens sheets can achieve simultaneous vertical and horizontal parallax. While automultiscopic displays realized with lenses are brighter than barrier designs, lens-based designs reduce spatial resolution; as a result, we seek to address the limitations of automultiscopic displays, particularly diminished brightness, reduced spatial resolution, and limited depth of field using emerging multilayer architectures.

Depth of field is a key metric for judging the relative performance of various automultiscopic display technologies. As described by Zwicker *et al.* [3], the *depth of field* of an automultiscopic display is an expression describing the maximum spatial frequency that can be depicted, without aliasing, in a virtual plane oriented parallel to, and located a known distance from, the display surface. In this paper, we derive upper bounds on the spatio-angular bandwidth for any

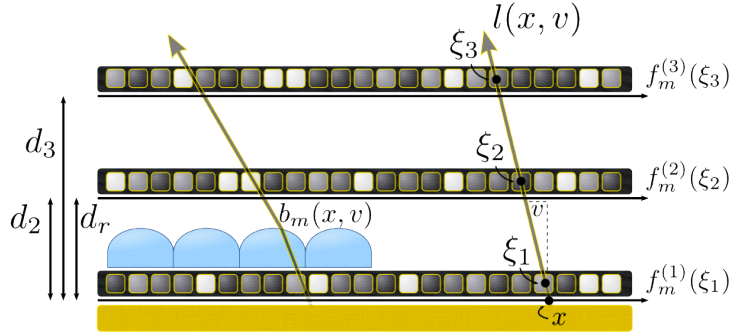


**Figure 1.** Tensor displays. A stack of  $N$  light-attenuating layers is illuminated by a uniform or directional backlight (e.g., depicted above as a lenslet array affixed to the rear display layer). A time-multiplexed sequence of  $M$  patterns, with transmittance  $f_m^{(n)}(\xi_n)$  at point  $\xi_n$  on layer  $n$  during frame  $m$ , are rapidly displayed such that an observer perceives the time average. The emitted light field  $l(x, v)$  is defined using a relative two-plane parameterization, where  $v$  denotes the point of intersection of the ray  $(x, v)$  with a plane located a distance  $d_r$  from the  $x$ -axis. The directional backlight emits a low-resolution light field  $b_m(x, v)$  during frame  $m$ .

multilayer, attenuation-based display incorporating either uniform or directional backlighting [4]. This upper bound is shown, for two layers, to encompass prior depth of field expressions for parallax barriers and integral imaging. Most significantly, the upper bound indicates multilayer, attenuation-based displays can significantly increase the spatial resolution for virtual objects located close to the display surface, as compared to current architectures.

Automultiscopic display systems must optimize their performance by considering three components: multiview content, display elements, and viewers. Prior works consider the benefits of pre-filtering multiview content for a particular display device [5]. Others consider adapting display elements (e.g., the spacing within parallax barriers) depending on viewer position [6, 7]. We propose four generalizations of conventional parallax barriers: *High-Rank 3D (HR3D)* [8], *Layered 3D* [9], *Polarization Fields* [10], and *Tensor Displays* [11], for which display elements are optimized for the multiview content. As shown in Figure 1 and recently reviewed by Lanman *et al.* [12], such displays comprise stacks of time-multiplexed, light-attenuating (or polarization-rotating) layers (e.g., multilayer LCDs). The resulting generalized barriers significantly differ from existing heuristics (e.g., grids of slits or pinholes) and achieve increased optical transmission, enhanced spatial resolution, greater depth of field, and higher refresh rates, while preserving the fidelity of displayed images. Most significantly, displays employing these generalized, multilayer barrier architectures can similarly benefit from pre-filtered multiview content and can adapt to the viewer position, allowing simultaneous optimization of all three system components.

In this paper, we present a signal-processing framework for comparing the depths of field for conventional automultiscopic displays and emerging architectures comprising multiple light-attenuating layers. Section 2 assesses the depth of field for conventional designs. In Sections 3 and 4, we derive upper bounds for the depth of field for any multilayer attenuation-based display illuminated with uniform or directional backlighting, respectively. In Section 5, we compare these upper bounds to formally establish the benefits of multilayer automultiscopic displays.

## 2. Depth of Field for Conventional Automultiscopic Displays

As described by Zwicker *et al.* [3], the depth of field of an automultiscopic display is an expression describing the maximum spatial frequency  $\omega_{\xi_{\max}}$  that can be depicted, without aliasing, in a virtual plane oriented parallel to, and located a distance  $d_o$  from, the middle of the display enclosure (see Figure 1). As established in that work, the depth of field can be assessed by

analyzing the spectral properties of the emitted light field. For conventional parallax barriers and integral imaging, the discrete sampling of emitted rays  $(x, v)$  produces a light field spectrum  $\hat{l}(\omega_x, \omega_v)$  that is non-zero only within a rectangle, where  $\omega_x$  and  $\omega_v$  are the spatial and angular frequencies, respectively. As described by Chai *et al.* [13] and Durand *et al.* [14], the spectrum of a diffuse surface, located at distance  $d_o$ , corresponds to the line  $\omega_v = (d_o/d_r)\omega_x$  in the frequency domain, where  $d_r$  is the distance between the  $x$ -axis and  $v$ -axis. The spatial cutoff frequency  $\omega_{\xi_{\max}}$  is given by the intersection of this line with the spectral bandwidth of the display.

Consider the emitted light field spectrum for a parallax barrier or integral imaging display. Let  $\Delta x$  denote the spatial sampling rate (i.e., the spacing between barrier slits, pinholes, or lenslets). Similarly, let  $\Delta v$  denote the angular sampling rate; for a conventional automultiscopic display with field of view  $\alpha$  and  $A$  distinct views, the angular sampling rate  $\Delta v = (2d_r/A)\tan(\alpha/2)$ . Thus, the light field spectrum for a conventional automultiscopic display is non-zero only for  $|\omega_x| \leq 1/(2\Delta x)$  and  $|\omega_v| \leq 1/(2\Delta v)$ . Intersecting the line  $\omega_v = (d_o/d_r)\omega_x$  with this rectangular region yields the following expression for the depth of field.

$$\omega_{\xi_{\max}}(d_o) = \begin{cases} \frac{1}{2\Delta x} & \text{for } |d_o| \leq d_r(\frac{\Delta x}{\Delta v}), \\ \frac{d_r}{2|d_o|\Delta v} & \text{otherwise} \end{cases} \quad (1)$$

This expression supports the following intuition: near the display (i.e., for  $|d_o| \leq d_r(\Delta x/\Delta v)$ ), the maximum spatial frequency that can be depicted in a virtual plane, separated by  $d_o$ , is limited by the spacing  $\Delta x$  between slits, pinholes, or lenslets. Far from the display, however, the maximum spatial frequency is limited by the angular sampling rate  $\Delta v$  and is independent of the spacing between the slits, pinholes, or lenslets.

### 3. Depth of Field for Multilayer Displays with Uniform Backlighting

The upper bound on the depth of field for a *static* multilayer display with uniform backlighting (i.e., one for which the layer patterns do not vary over time) is similarly assessed by considering the maximum spectral bandwidth, for all possible layer patterns. The light field  $l(x, v)$  emitted by an  $N$ -layer display with uniform backlighting is given by

$$l(x, v) = \prod_{n=1}^N f^{(n)}(x + (d_n/d_r)v), \quad (2)$$

where  $f^{(n)}(\xi_n) \in [0, 1]$  is the transmittance at the point  $\xi_n$  of layer  $n$ , separated a distance  $d_n$  from the  $x$ -axis (see Figure 1). The 2D Fourier transform of this expression is given by

$$\hat{l}(\omega_x, \omega_v) = \int_{-\infty}^{\infty} \int_{-\infty}^{\infty} \prod_{n=1}^N f^{(n)}(x + (d_n/d_r)v) e^{-2\pi j\omega_x x} e^{-2\pi j\omega_v v} dx dv. \quad (3)$$

By the convolution property of Fourier transforms [15], this expression reduces to a *repeated convolution* of the individual layer spectra  $\hat{f}^{(n)}(\omega_x, \omega_v)$ , such that the light field spectrum  $\hat{l}(\omega_x, \omega_v)$  is given by

$$\hat{l}(\omega_x, \omega_v) = \underset{n=1}{\overset{N}{*}} \hat{f}^{(n)}(\omega_x) \delta(\omega_v - (d_n/d_r)\omega_x), \quad (4)$$

where  $*$  denotes convolution and the repeated convolution operator is defined as

$$\underset{n=1}{\overset{N}{*}} \hat{f}^{(n)}(\omega_x, \omega_v) \equiv \hat{f}^{(1)}(\omega_x, \omega_v) * \hat{f}^{(2)}(\omega_x, \omega_v) * \dots * \hat{f}^{(N)}(\omega_x, \omega_v). \quad (5)$$

Note that each layer produces a spectrum  $\hat{f}^{(n)}(\omega_x, \omega_v) = \hat{f}^{(n)}(\omega_x) \delta(\omega_v - (d_n/d_r)\omega_x)$  that lies along the line  $\omega_v = (d_n/d_r)\omega_x$ , following Chai *et al.* [13]. Since each layer has a finite resolution, the layer spectra  $\hat{f}^{(n)}(\omega_x)$  are non-zero only for  $|\omega_x| \leq \omega_0 = 1/(2p)$ , where  $p$  is the pixel pitch.

In the preceding analysis we have focused on static multilayer displays. A *dynamic* multilayer display exploits rapid temporal modulation, such that an observer perceives the average of an  $M$ -frame sequence. Generalizing Equation 2, the emitted light field  $l(x, v)$  is given by

$$l(x, v) = \frac{1}{M} \sum_{m=1}^M \prod_{n=1}^N f_m^{(n)}(x + (d_n/d_r)v), \quad (6)$$

where  $f_m^{(n)}(\xi_n)$  is the transmittance at the point  $\xi_n$  of layer  $n$  during frame  $m$ . Note that, by the linearity property of the Fourier transform, the inclusion of time multiplexing does not alter the maximum spectral support for a given multilayer display configuration. That is, both static and dynamic multilayer displays have identical spectral bandwidths. Yet, as established by Wetzstein *et al.* [11], the added degrees of freedom afforded by temporal multiplexing allow dynamic multilayer displays to more closely approach the upper bound on the depth of field.

### 3.1. Two-Layer Displays with Uniform Backlighting

Consider a two-layer display with uniform backlighting, with the layers separated by a distance  $\Delta d$  and  $\omega_0 = 1/(2p)$  denoting the spatial cutoff frequency for each layer with pixel pitch  $p$ . Equation 4 yields the following analytic expression for the light field spectrum  $\hat{l}(\omega_x, \omega_v)$ .

$$\hat{l}(\omega_x, \omega_v) = \hat{f}^{(1)}(\omega_x) \delta(\omega_v + (\Delta d/(2d_r))\omega_x) * \hat{f}^{(2)}(\omega_x) \delta(\omega_v - (\Delta d/(2d_r))\omega_x) \quad (7)$$

As shown in Figure 2, a diamond-shaped region encloses the non-zero spectral support for any two-layer display. This region is bounded by a rectangle, such that  $|\omega_x| \leq 2\omega_0$  and  $|\omega_v| \leq (\Delta d/d_r)\omega_0$ . The spatial cutoff frequency  $\omega_{\xi_{\max}}$  is again found by intersecting the line  $\omega_v = (d_o/d_r)\omega_x$  with the boundary of the maximum-achievable spectral support. This geometric construction yields the following upper bound on the depth of field for any two-layer display.

$$\omega_{\xi_{\max}}(d_o) = \left( \frac{2\Delta d}{\Delta d + 2|d_o|} \right) \omega_0 \quad (8)$$

Note that this expression is equivalent to that previously derived for two-layer displays by Wetzstein *et al.* [9].

### 3.2. Three-Layer Displays with Uniform Backlighting

Equation 4 yields the following analytic expression for the light field spectrum  $\hat{l}(\omega_x, \omega_v)$  for any three-layer display, with layers separated by a distance  $\Delta d$ .

$$\hat{l}(\omega_x, \omega_v) = \hat{f}^{(1)}(\omega_x) \delta(\omega_v + (\Delta d/d_r)\omega_x) * \hat{f}^{(2)}(\omega_x) \delta(\omega_v) * \hat{f}^{(3)}(\omega_x) \delta(\omega_v - (\Delta d/d_r)\omega_x) \quad (9)$$

As shown in Figure 2, a hexagonal region encloses the non-zero spectral support for any three-layer display. This region is bounded by a rectangle, such that  $|\omega_x| \leq 3\omega_0$  and  $|\omega_v| \leq 2(\Delta d/d_r)\omega_0$ . Intersecting the line  $\omega_v = (d_o/d_r)\omega_x$  with the boundary of the maximum-achievable spectral support again yields the following upper bound on the depth of field.

$$\omega_{\xi_{\max}}(d_o) = \begin{cases} \left( \frac{3\Delta d}{\Delta d + |d_o|} \right) \omega_0 & \text{for } |d_o| \leq 2\Delta d, \\ \left( \frac{2\Delta d}{|d_o|} \right) \omega_0 & \text{otherwise} \end{cases} \quad (10)$$

As shown in Figure 2, the bandwidth for three-layer displays exceeds that for either conventional or two-layer architectures, motivating the development of multilayer displays for extended depth of field. Note that, using the geometric construction outlined for two-layer and three-layer displays, one may derive an analytic upper bound for an arbitrary number of layers.

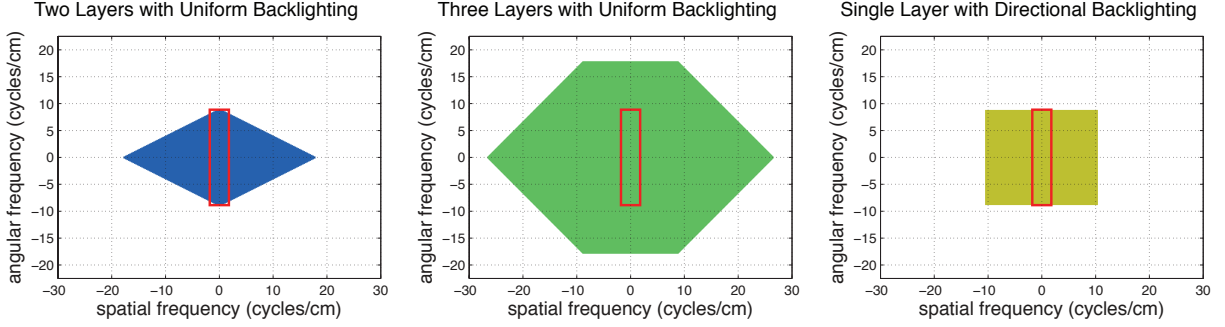


**Figure 2.** Spectral support for multilayer displays with uniform and directional backlighting. The spectral support is illustrated for two-layer and three-layer displays with uniform backlighting, shaded blue and green, on the left and in the middle, respectively. The spectral support for a single-layer display with directional backlighting is shaded yellow on the right. The spectral support for a conventional light field display (e.g., parallax barriers or integral imaging) is denoted by the red box. Display parameters correspond to those used for the prototype *Tensor Displays* described by Wetzstein *et al.* [11]. Specifically, multiple LCD panels, each with pixel pitch  $p = 0.6$  mm, are separated by a distance of  $\Delta d = 8$  mm.

### 3.3. General Multilayer Displays with Uniform Backlighting

For an  $N$ -layer display, a direct geometric construction for the upper bound on the depth of field becomes cumbersome. As an alternative, we apply the central limit theorem [16] to obtain an approximate expression for the spectral support due to the repeated convolutions in Equation 4; as derived by Chaudhury *et al.* [17], the repeated convolution of  $N$  two-dimensional spectra, each with mean  $\mu_n = [0, 0]$  and covariance matrix  $\Sigma_n$ , tends to a bivariate Gaussian distribution:

$$\hat{l}(\omega_x, \omega_v) \approx \left( \frac{1}{2\pi|\Sigma|^{\frac{1}{2}}} \right) \exp\left(-\frac{1}{2}\omega^\top \Sigma^{-1}\omega\right), \text{ for } \Sigma = \sum_{n=1}^N \Sigma_n, \quad (11)$$

where  $\omega = [\omega_x, \omega_v]$  is a given spatio-angular frequency.

In the following analysis, we define the the maximum bandwidth for any given layer as follows.

$$\hat{f}^{(n)}(\omega_x, \omega_v) \equiv \begin{cases} \frac{1}{2\epsilon\omega_0} & \text{for } |\omega_x| \leq \omega_0 \text{ and } |\omega_v - (d_n/d_r)\omega_x| \leq \frac{\epsilon}{2} \\ 0 & \text{otherwise} \end{cases} \quad (12)$$

This definition corresponds to a thin layer with a spatially-varying transmittance characterized by a white noise process (i.e., a uniform spectral energy density) [18]. Note that the spectrum of a layer located at a distance  $d_n$  will be non-zero along a single line, with slope  $d_n/d_r$ , only in the limit as  $\epsilon$  tends to zero. Under this definition for the patterns depicted with an  $N$ -layer display, the cumulative mean spatio-angular frequency  $\mu = \mu_n = 0$ , since each layer spectrum is symmetric about the origin. Similarly, the covariance matrix  $\Sigma_n$  for each layer is given by

$$\Sigma_n = \begin{bmatrix} \int_{-\infty}^{\infty} \int_{-\infty}^{\infty} \omega_x^2 \hat{f}^{(n)}(\omega_x, \omega_v) d\omega_x d\omega_v & \int_{-\infty}^{\infty} \int_{-\infty}^{\infty} \omega_x \omega_v \hat{f}^{(n)}(\omega_x, \omega_v) d\omega_x d\omega_v \\ \int_{-\infty}^{\infty} \int_{-\infty}^{\infty} \omega_x \omega_v \hat{f}^{(n)}(\omega_x, \omega_v) d\omega_x d\omega_v & \int_{-\infty}^{\infty} \int_{-\infty}^{\infty} \omega_v^2 \hat{f}^{(n)}(\omega_x, \omega_v) d\omega_x d\omega_v \end{bmatrix}. \quad (13)$$

Substituting Equation 12 yields the covariance matrix:

$$\lim_{\epsilon \rightarrow 0} \Sigma_n = \frac{\omega_0^2}{3} \begin{bmatrix} 1 & \frac{d_n}{d_r} \\ \frac{d_n}{d_r} & \left(\frac{d_n}{d_r}\right)^2 \end{bmatrix}, \quad (14)$$

where the limit of  $\epsilon$  tending to zero corresponds to an infinitesimally-thin layer. Thus, the cumulative covariance matrix  $\Sigma$  of the light field spectrum is approximated by the summation:

$$\Sigma = \sum_{n=1}^N \Sigma_n = \begin{bmatrix} \sigma_{\omega_x}^2 & 0 \\ 0 & \sigma_{\omega_v}^2 \end{bmatrix} = \frac{\omega_0^2}{3} \begin{bmatrix} N & 0 \\ 0 & \left(\frac{N(N^2-1)}{12}\right) \left(\frac{\Delta d}{d_r}\right)^2 \end{bmatrix}, \quad (15)$$

for layers uniformly-spaced on the interval  $d_n \in [-(N-1)\Delta d/2, (N-1)\Delta d/2]$ . Substituting into Equation 11 yields the following approximation for the spectrum of an  $N$ -layer display.

$$\hat{l}(\omega_x, \omega_v) \approx \left( \frac{1}{2\pi\sigma_{\omega_x}\sigma_{\omega_v}} \right) \exp\left( -\frac{\omega_x^2}{2\sigma_{\omega_x}^2} - \frac{\omega_v^2}{2\sigma_{\omega_v}^2} \right) \quad (16)$$

Equation 16 can be used to approximate the upper bound on the depth of field, depending on the number of layers  $N$ , the separation distance  $\Delta d$  between layers, and the layer cutoff frequency  $\omega_0 = 1/2p$ . Under this model, the spectral support of a multilayer display is approximated by a bivariate Gaussian; curves defining spatio-angular frequencies with equal modulation energies correspond to ellipses, such that

$$\frac{\omega_x^2}{\sigma_{\omega_x}^2} + \frac{\omega_v^2}{\sigma_{\omega_v}^2} = \lambda^2, \quad (17)$$

where  $\pm\lambda\sigma_{\omega_x}$  and  $\pm\lambda\sigma_{\omega_v}$  are the points of intersection with the  $\omega_x$ -axis and  $\omega_v$ -axis, respectively. One can obtain an approximate upper bound on the depth of field, for an arbitrary number of layers, by finding the intersection of the line  $\omega_v = (d_o/d_r)\omega_x$  with the ellipse corresponding to the highest spatial frequency achievable by an  $N$ -layer display. From Equations 4 and 12, the repeated convolution of  $N$  layers, each extending over  $\pm\omega_0$  along the  $\omega_x$ -axis, will produce non-zero spatial frequencies within the region  $|\omega_x| \leq N\omega_0$ . Thus, the ellipse with  $\lambda = N\omega_0/\sigma_{\omega_x}$  provides the following approximate upper bound on the depth of field for an  $N$ -layer display.

$$|f_\xi| \leq N\omega_0 \sqrt{\frac{(N^2-1)\Delta d^2}{(N^2-1)\Delta d^2 + 12d_o^2}} \quad (18)$$

This expression approximates the upper bound on the depth of field for two-layer and three-layer displays, given exactly by Equations 8 and 10, respectively. A comparison of the upper bound for multilayer vs. conventional automultiscopic displays is shown in Figure 3. Note that additional layers significantly increase the upper bound on the achievable spatial resolution, which is expected due to repeated convolution of layer spectra via Equation 4. In summary, these upper bounds indicate the theoretical origin for the increased depth of field observed with recent multilayer display architectures, including *HR3D* [8], *Layered 3D* [9], *Polarization Fields* [10], and *Tensor Displays* [11].

#### 4. Depth of Field for Multilayer Displays with Directional Backlighting

The upper bound on the depth of field for a multilayer display with directional backlighting is assessed, similar to Section 3, by considering the maximum spectral bandwidth, for all possible layer and backlight illumination patterns. Generalizing Equation 2 yields a model for the emitted light field  $l(x, v)$  of an  $N$ -layer display with directional backlighting, such that

$$l(x, v) = b(x, v) \prod_{n=1}^N f^{(n)}(x + (d_n/d_r)v), \quad (19)$$

where  $b(x, v)$  denotes the light field emitted by the directional backlight. We consider directional backlighting to be equivalent to any low-resolution light field display placed behind a stack of

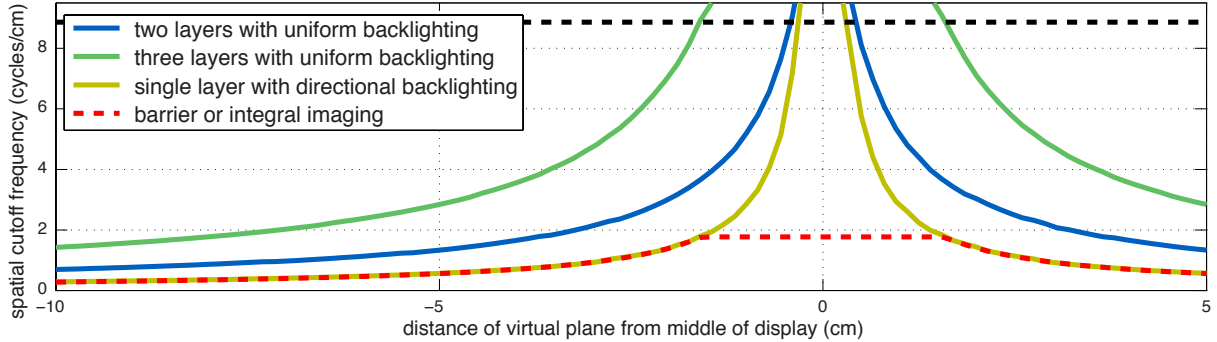


**Figure 3.** Comparison of the upper bound on the depth of field for conventional light field displays (red), two-layer (blue) and three-layer (green) displays with uniform backlighting, and single-layer displays with directional backlighting (yellow). The dashed black line denotes the spatial cutoff frequency  $\omega_0$  for each layer. Display parameters correspond to those in Figure 2.

light-attenuating layers. For example, as shown in Figure 1, such directional backlighting may comprise an integral imaging display, for which one desires to enhance the spatial resolution of the emitted light field. As before, the 2D Fourier transform of this expression is given by

$$\hat{l}(\omega_x, \omega_v) = \int_{-\infty}^{\infty} \int_{-\infty}^{\infty} b(x, v) \prod_{n=1}^N f^{(n)}(x + (d_n/d_r)v) e^{-2\pi j\omega_x x} e^{-2\pi j\omega_v v} dx dv, \quad (20)$$

yielding the following emitted light field spectrum:

$$\hat{l}(\omega_x, \omega_v) = \hat{b}(\omega_x, \omega_v) * \left[ \underset{n=1}{*} \hat{f}^{(n)}(\omega_x) \delta(\omega_v - (d_n/d_r)\omega_x) \right]. \quad (21)$$

#### 4.1. Single-Layer Displays with Directional Backlighting

In this section, we consider a single-layer display with directional backlighting; for example, Wetzstein *et al.* [11] describe a prototype consisting of a single LCD panel placed directly on top of an integral imaging display, comprising a lenslet array affixed to a second LCD panel. Consistent with that prototype, we assume that the directional backlight implements a low-resolution light field display, such that  $\hat{b}(\omega_x, \omega_v)$  has non-zero support for  $|\omega_x| \leq 1/(2\Delta x)$  and  $|\omega_v| \leq 1/(2\Delta v)$  (i.e., the red boxes in Figure 2). Equation 21 yields the following analytic expression for the light field spectrum.

$$\hat{l}(\omega_x, \omega_v) = \hat{b}(\omega_x, \omega_v) * \hat{f}(\omega_x) \delta(\omega_v) \quad (22)$$

Note that the layer spectrum  $\hat{f}(\omega_x, \omega_v) = \hat{f}(\omega_x) \delta(\omega_v)$  is constrained to a horizontal line of width  $|\omega_x| \leq \omega_0$ . Thus, convolution with the directional backlight spectrum results in an extended rectangular spectral support exceeding that of a conventional light field display; as shown in Figure 2, the rectangular region is given by  $|\omega_x| \leq 1/(2\Delta x) + \omega_0$  and  $|\omega_v| \leq 1/(2\Delta v)$ . Note that placing a light-attenuating layer directly on top of a conventional light field display only increases the spatial resolution; the angular resolution of the underlying low-resolution light field display is preserved. Intersecting the line  $\omega_v = (d_o/d_r)\omega_x$  with the boundary of the maximum-achievable spectral support yields the following upper bound on the depth of field.

$$\omega_{\xi_{\max}}(d_o) = \begin{cases} \frac{1}{2\Delta x} + \omega_0 & \text{for } |d_o| \leq d_r \left( \frac{\Delta x}{\Delta v + 2\Delta x \Delta v \omega_0} \right), \\ \frac{d_r}{2|d_o| \Delta v} & \text{otherwise} \end{cases} \quad (23)$$

As shown in Figure 3, the addition of a single light-attenuating layer significantly increases the spatial resolution near the display surface, as compared to a conventional parallax barrier or integral imaging display. However, far from the display, the upper bound on the depth of field is identical to these conventional automultiscopic displays.

## 5. Conclusion

Our analysis indicates a promising application for multilayer automultiscopic displays: increased depth of field can be achieved by covering any low-resolution light field display with time-multiplexed, light-attenuating layers. In this analysis, we assume continuously-varying layer transmittances; a promising research direction is to characterize the upper bounds with discrete pixels. However, with the presented analysis, we observe that static and dynamic multilayer displays have identical spectral supports (i.e., averaging over an  $M$ -frame sequence does not alter the maximum-achievable bandwidth). Yet, as observed by Lanman *et al.* [8] and Wetzstein *et al.* [11], time multiplexing significantly reduces artifacts occurring with static multilayer designs. We attribute this to the additional degrees of freedom allowed with time multiplexing. While the upper bounds may be identical, in practice this bound cannot be achieved with static methods, motivating multilayer automultiscopic displays for joint multilayer, multiframe decompositions capable of approaching the upper bound—significantly extending the depth of field achievable using current-generation display technologies, including LCD panels.

## Acknowledgments

We recognize the support of the Camera Culture group and the MIT Media Lab sponsors. Douglas Lanman was supported by NSF Grant IIS-1116452 and by the DARPA MOSAIC program. Gordon Wetzstein was supported by the DARPA SCENICC program. Ramesh Raskar was supported by an Alfred P. Sloan Research Fellowship and a DARPA Young Faculty Award.

## References

- [1] Ives F E 1903 Parallax stereogram and process of making same U.S. Patent 725,567
- [2] Lippmann G 1908 *Journal of Physics* **7** 821–825
- [3] Zwicker M, Matusik W, Durand F and Pfister H 2006 *Eurographics Symposium on Rendering*
- [4] Urey H, Chellappan K V, Erden E and Surman P 2011 *Proc. IEEE* **99** 540–555
- [5] Zwicker M, Vetro A, Yea S, Matusik W, Pfister H and Durand F 2007 *IEEE Signal Processing* **24** 88–96
- [6] Perlin K, Paxia S and Kollin J S 2000 *SIGGRAPH* (ACM) pp 319–326
- [7] Peterka T, Kooima R L, Sandin D J, Johnson A, Leigh J and DeFanti T A 2008 *IEEE Transactions on Visualization and Computer Graphics* **14** 487–499
- [8] Lanman D, Hirsch M, Kim Y and Raskar R 2010 *ACM Trans. Graph.* **29**(6) 163:1–163:10
- [9] Wetzstein G, Lanman D, Heidrich W and Raskar R 2011 *ACM Trans. Graph.* **30**(4) 1–11
- [10] Lanman D, Wetzstein G, Hirsch M, Heidrich W and Raskar R 2011 *ACM Trans. Graph.* **3**(6) 1–9
- [11] Wetzstein G, Lanman D, Hirsch M and Raskar R 2012 *ACM Trans. Graph.* **31** 1–11
- [12] Lanman D, Wetzstein G, Hirsch M, Heidrich W and Raskar R 2012 *SPIE Stereoscopic Displays and Applications XXIII* vol 8288 pp 82880A–1– 82880A–13
- [13] Chai J X, Tong X, Chan S C and Shum H Y 2000 *SIGGRAPH* (ACM) pp 307–318
- [14] Durand F, Holzschuch N, Soler C, Chan E and Sillion F X 2005 *ACM Trans. Graph.* **24** 1115–1126
- [15] Bracewell R 1999 *The Fourier Transform and Its Applications* (McGraw-Hill)
- [16] Peebles P 2000 *Probability, Random Variables, and Random Signal Principles* (McGraw-Hill)
- [17] Chaudhury K N, Muñoz-Barrutia A and Unser M 2010 *IEEE Trans. Image* **19** 2290–2306
- [18] Haykin S 2000 *Communication Systems* (Wiley)